ORIGINAL ARTICLE

A novel study on the stepwise electrodeposition approach for the synthesis of Pd based nanoparticles, characterization and their enhanced electrooxidation activities

Caglar Avci[1]; Fazile Cicek[1]; Hilal Celik Kazici[1]; Arif Kivrak[2]; Hilal Kivrak[1,]*

[1]Chemical Engineering Department, Van Yüzüncü Yil University, Van, 65000, Turkey
[2]Department of Chemistry, Van Yüzüncü Yil University, Van, 65000, Turkey

Abstract
Herein, a stepwise electrodeposition technique was used to synthesize the Pd based nanoparticles on indium-tin oxide (ITO) electrodes. First of all, Pd nanoparticles were electrodeposited on ITO via one step electrodeposition technique. Furthermore, Au was electrodeposited on Pd. Finally, Co was electrodeposited on Au and Pd electrodeposited ITO electrode via stepwise electrodeposition technique. Characterization of these electrodes was performed by x-ray diffraction (XRD) and scanning electrode microscopy (SEM) techniques. Considering the XRD pattern, well-defined ITO peaks, Pd, and Au fcc structure peaks are clearly visible for Pd based electrodes. On the other hand, Co has two main crystal structures such as face-centered-cubic (fcc) and hexagonal close-packed (hcp) phases. SEM images illustrates that spherical particles were obtained for these Pd based electrodes. Finally, formic acid electrooxidation activities of these electrodes were evaluated and enhanced electrooxidation activities were obtained.

Keywords: *Au; Co; Electrodeposition; Nanoparticles; Pd; Trimetallic, ITO.*

INTRODUCTION

Polymer electrolyte membrane (PEM) based fuel cells are generally considered as a promising alternative to batteries in portable power devices. Conventionally, hydrogen fuel cells (H_2-PEM) and direct methanol fuel cells (DMFCs) have gained intensive research interest [1-3]. The critical limitations for commercialization of H_2-PEM are the high cost of miniaturized H_2 containers, potential dangers in transportation and use of H_2, and low gas-phase energy density of H_2. Hence, direct formic acid fuel cells (DFAFCs) have recently attracted tremendous research interest as potential power sources [1-8]. Formic acid (FA, HCOOH) is a pleased alternative fuel due to its higher energy density, stability, less toxicity, and lower crossover through nafion membrane than CH_3OH [9].

The dehydration of FA to form the CO poisoning is facile on Pt surfaces, which drastically impedes the dehydrogenation at lower potentials. Toxic carbon monoxide (CO) produced by dehydration of FA significantly reduces the activity of Pt catalyst in PEMFC [9]. In contrast, the dehydrogenation of FA to form CO_2 prevails on Pd surfaces. Thus, Pd catalysts exhibit superior performances for the formic acid electrooxidation (FAEO) compared with Pt catalysts, because FAEO mainly proceeds through a direct dehydrogenation reaction mechanism on Pd catalyst to form CO_2 with generating less poisoning species [5, 10-17]. However, monometallic Pd is readily deactivated due to adsorption of poisonous CO resulting from the reduction of CO_2 at H-adsorbed Pd surfaces. Therefore, the development of new Pd based catalysts with improved activity and stability has great importance for the practical applications of DFAFC systems. Pd and Pd-based materials have attracted a lot of attention due to their superior catalytic activities on FAEO [5, 11-13].

* Corresponding Author Email: *hilalkivrak@gmail.com*

The incorporation of secondary metal has better CO resistance than Pd, seems to be a promising solution to avoid CO-deactivation of Pd active sites. Furthermore, Du *et al.* has also found that PdNi alloy nanowires are highly active catalysts for the FAEO [14]. PdAu supported on functionalized graphene nanoplates revealed better activity than Pd/C catalysts displayed [15]. Jiang and coworkers reported that Ag@Pd core@shell nanotube catalysts exhibit better CO tolerance and activity than Pd catalyst [16]. In conclusion, as has been mentioned before, Pd-based multimetallic catalysts demonstrate an improved electrochemical activity and stability toward FAEO. Furthermore, the cost of the Pd-based catalysts can be reduced employing less amount of Pd in the catalyst synthesis when multimetallic catalysts used.

This study indicates that Co doping in PdAg bimetallic NPs can significantly improve its FAO activity [17]. Wang *et al.* reported that CoAuPd nano alloy is a very efficient catalyst for FA dehydrogenation [6]. As mentioned earlier, FAEO proceeds through FA dehydrogenation on anode catalyst. It is found that the trimetallic Pd-based nanoalloys are more flexible than the corresponding bimetallic alloys in tuning the composition and electronic properties of catalytic surfaces. Moreover, the fabrication of Pd-based ternary nanoalloys is also beneficial to maximize the utilization of Pd in the catalysts as well as to enhance their electrocatalytic properties. Consequently, it is of great importance to design a trimetallic Pd-based alloy with low cost and high performance as an electrocatalyst for FAEO. As has been mentioned above, FAEO proceeds through FA dehydrogenation, thus FA catalysts could enhance FAEO activity. At present, CoAuPd catalysts were prepared with a novel electrochemical deposition method and their FAEO activities method.

The direct electrochemical deposition method is advantageous over the traditional synthetic techniques due to the simplicity of electrochemical deposition parameters (current, voltage, time, etc.). The latter method has a poor control over the composition and structures of NPs. A conductive solid support is essential for electrodeposition. ITO has a very low background current and large electrochemical potential window [18-20]. Hence, it is a cheap substitute for the gold and the glassy carbon electrode, and an ideal substrate for electrocatalytic research into NPs. Kim *et al.* reported that electrochemically deposited Pd NPs on indium-tin oxide (ITO) exhibited enhanced electrocatalytic activity [21].

Objective of this research is to show CoAuPd catalyst exhibiting enhanced FAEO activity. Herein, we present a facile synthesis of Pd, Pd-Au, and CoAuPd by means of electrochemical deposition technique on ITO electrode. The electrochemical depositions of Pd, Pd-Au, and CoAuPd on ITO electrodes were performed by CV at 10 mV s^{-1} scan rate, and FAEO activities of these monometallic, bimetallic, and trimetallic electrodes were examined by CV, CA (chronoamperometry) techniques.

EXPERIMENTAL

Preparation of Electrodes

$PdCl_2$, $AuCl$, $CoCl_2$, H_2SO_4, HCl and formic acid and ITO electrodes were purchased from Sigma-Aldrich. The electrochemical deposition experiments were performed using a CHI660 electrochemical analyzer. A platinum wire and an Ag/AgCl were the counter and reference electrodes, respectively. Electrochemical deposition was performed on ITO working electrode. The area of the working electrode was 0.28 cm^2. Prior to each electro-deposition, the ITO surfaces were cleaned in an ultrasonic ethanol bath (for 5 min) in order to remove any impurity. Finally, they were rinsed in an ultrasonic pure water bath (for 5 min) and dried for 1 min using a N_2 stream. Then, Pd was electrodeposited on ITO electrodes by CV with a 0.1 M H_2SO_4 + 0.1 mM $PdCl_2$ + 0.2 mM HCl solution at 10 mV s^{-1} scan rate to prepare Pd/ITO electrode. On the other hand, Au was electrochemically deposition on ITO electrode in 0.1 M H_2SO_4 + 0.03 mM AuCl + 0.2 mM HCl solution by CV technique. Co was electrodeposited on ITO electrode from aqueous solutions containing 1 M H_2SO_4 + 0.01 mM $CoCl_2$ + 0.2 mM HCl by CV at a scan rate of 10 mVs^{-1}.

To prepare AuPd/ITO electrodes, Au was electrodeposited on ITO by CV at 10 mVs^{-1} with a 0.1 M H_2SO_4 + 0.03 mM AuCl + 0.2 mM HCl solution. Afterwards, Pd electrodeposition was tested on Au/ITO electrode by CV with a 0.1 M H_2SO_4 + 0.1 mM $PdCl_2$ + 0.2 mM HCl solution at 10 mVs^{-1} scan rate.

Three-step electro-deposition process was employed for the preparation of CoAuPd/ITO electrodes. Firstly, Co was electrodeposited on ITO electrode from aqueous solutions containing 1 M H_2SO_4 + 0.01 mM $CoCl_2$ + 0.2 mM HCl by CV at a scan rate of 10 mV s^{-1}. Then, Au was electrodeposited on Co/ITO electrode in 0.1 M H_2SO_4. Finally, Pd was electrodeposited on CoAu/ITO electrode.

Physical Characterization of Electrodes

Physical characterization of the Pd/ITO, AuPd/ITO and CoAuPd/ITO electrodes were performed by XRD and SEM. X-ray diffraction (XRD) patterns of the Pd/ITO, AuPd/ITO and CoAuPd/ITO electrodes were recorded between 2θ = 20.0–90.0° with 0.05° intervals on a Bruker D8 Advance X-ray diffractometer using (Cu-Kα λ = 1.5405 A°) as a radiation source. Further study was performed in a JEOL 5600LV scanning electron microscope (SEM) in back-scattered electrons (BEI), which is a compositional sensitive imaging mode. The morphology of Pd/ITO, AuPd/ITO and CoAuPd/ITO electrodes was characterized by SEM

Electrochemical measurements

CV and CA techniques were employed to examine the FAEO activities of Pd/ITO, AuPd/ITO, and CoAuPd/ITO electrodes in 0.5 M H_2SO_4 + 1 M HCOOH. In all experiments, the electrolyte was previously saturated by nitrogen. Before each experiment, the electrode surface was activated in 0.5 M H_2SO_4. Cyclic voltammograms were recorded between -0.25 V and 1.0 V with a scan rate of 10 mVs^{-1} in 0.5M H_2SO_4 + 1M HCOOH at 25 °C. Chronoamperometry voltammograms were recorded in 0.5 M H_2SO_4 + 1 M HCOOH at 25°C solution. Moreover, CA was performed in 0.5M H_2SO_4 + 1M HCOOH solution at 0.2 V for 200 s with 1000 s pulse width and 2s quiet times.

RESULTS AND DISCUSSION

Pd was electrochemically deposited by CV at 10 mV s^{-1} scan rate at 3 cycle scan according to the procedure given in the literature [20]. The reduction current of Pd^{2+} to Pd was shown at 0.025 V (Fig. 1a). The current density at 0.025 V reflects the formation from Pd^{2+} to Pd NPs on ITO electrodes. Pd NPs were electrochemically deposited on ITO by increasing the cycle number of CV to 1 and 3 times at 10 mV s^{-1} scan rate (Fig. 1a). For the first scan, it was observed that reduction currents of Pd^{2+} were observed at 0.025 V, representing the formation of Pd NPs on the surface of the ITO electrodes. Nevertheless, one noticed that the peak shape and peak potentials changed for the second and third scans. After the first scan, the current density of Pd^{2+} was shifted from 0.025 to 0.027 V, ascribed that the electrochemical deposition conditions of Pd^{2+} were altered. For the first scan, the nucleation of Pd^{+2} nanoparticles occurs on the surface of ITO electrode. On the other hand, at the second and third scans Pd NPs continue to nucleate on the Pd/ITO electrode. Therefore, the peak at 0.027 V is the reduction peak of Pd^{2+} on Pd NPs. The current density on 0.19 V is the hydrogen evolution and palladium hydride formation peaks. Furthermore, current density at 0.45 V is the oxygen reduction peaks. At anodic section at 0.8-0.9 V, a broad stripping was observed. The existence of this peak was attributed to the Pd dissolution or Pd oxidation processes Oxygen reduction will always occur at a mass transport controlled rate on the surface of the depositing Pd [22-23]. Likewise, Au was electrochemically deposited on ITO via CV at 10 mV s^{-1} scan rate at 3 cycle scan. The reduction current of Au revealed at 0.03 V, indicating the formation of AuNPs on ITO electrodes (insert in Fig. 1b).

The reduction currents of Au were observed at 0.03 V at first scan and these currents for the second and third scan were observed 0.05 V and 0.07 V, respectively. As has been mentioned before, the current density of Au reduction was shifted from 0.03 to 0.07 V after the first scan due to altering conditions on the formation of Au NPs. Cyclic voltammogram of Pd electro-deposition on Au/ITO electrode is shown in Fig. 1d. The current of Pd reduction on Au/ITO electrode was shown at 0.05 V. One could note that Pd reduction potential shifted for PdAu/ITO electrode 0.025 V compared to Pd/ITO electrode, the peak potential of Pd deposition is moving positively. This can be explained by the easier nucleation of Pd on Au than on the ITO substrate. Hydrogen and oxygen evolution peaks were also clearly observed on Fig. 1d. To prepare CoAuPd/ITO electrode, firstly, Au^{+2} was electrodeposited on ITO electrode. Then, Co^{+2} was electrodeposited on Au/ITO electrode. Finally, electrochemical deposition of Pd^{+2} was performed on CoAu/ITO electrode. The cyclic voltammogram of Pd^{+2} electrodeposition was demonstrated on Fig. 1e. The reduction current of Pd was measured at -0.05 V for the Pd deposition on CoAu/ITO electrode, revealing that Pd nucleation on CoAu/ITO electrode is more difficult compared to Pd nucleation on ITO and Pd nucleation on Au/ITO electrode.

XRD results for Pd/ITO, AuPd/ITO, and CoAuPd/ITO electrodes were given in Fig. 2. One can clearly see that ITO peaks are well-defined. For ITO, it gives reflections only from (123), (400), (332) and (611) planes, revealing that bcc structure (JCPDS File No. 6- 416). The absence of reflections from
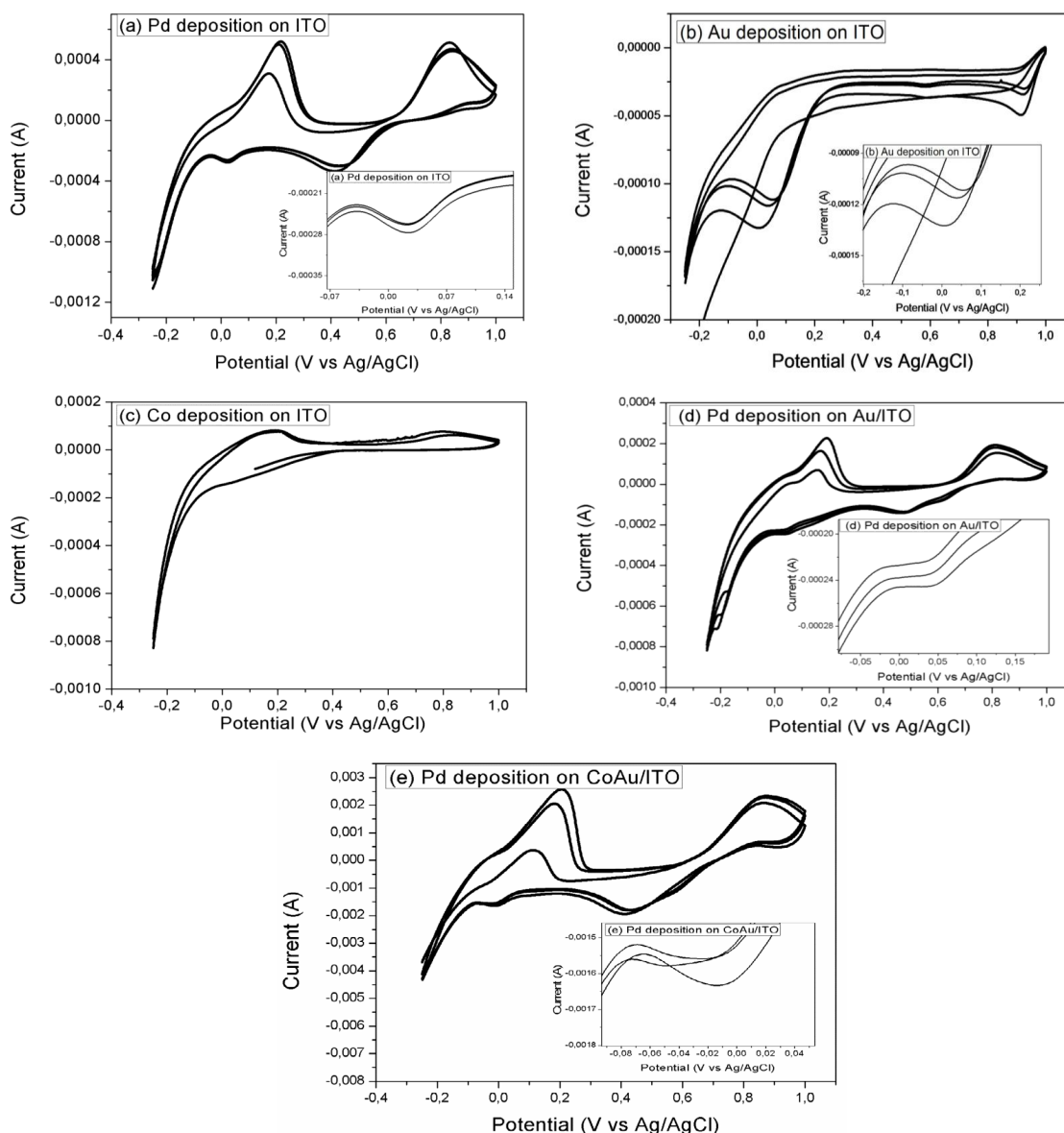
Fig. 1: CVs for (a) Pd electrochemical deposition on ITO, (b) Au electrochemical deposition on ITO, (c) Co electrodeposition on ITO, (d) Pd electrodeposition on Au/ITO, (e) Pd electrodeposition on CoAu/ITO electrodes at 10mVs⁻¹ scan rate.

(211), (322) and (431) plains of ITO, with smaller thickness are not due to the orientation, but due to the lack of sample thickness. On the other hand, Pd (111), (200), (220) and (311) planes, were observed on Fig. 2a, reveals the Pd face-centered cubic (fcc) structure (JCPDS card no 46-1043).

XRD characterization pattern of AuPd/ITO electrode is given in Fig. 2b. One can clearly see the well-defined ITO peaks. Furthermore, Pd and Au diffraction patterns show a fcc structural characterization. The XRD peak corresponding to the Au diffraction peaks of (2 2 0) were observed at

67°. XRD pattern of CoAuPd/ITO electrode is given in Fig. 2c. Both Pd and Au fcc structure peaks were observed on the XRD pattern of the CoAuPd/ITO electrode. Cobalt has two main crystal structures as; face-centered-cubic (fcc) and hexagonal close-packed (hcp) phases. The two phases of cobalt usually coexist at room temperature and are often difficult to be separated from each other. For FCC structured Co crystal phase, the diffraction peaks at 2ϑ values of 44°, 51°, 76°, 92° and 98° corresponds to (111), (200), (220), (311) and (222) crystal planes, which indicate formation of

fcc crystalline cobalt (JCPDS card no 15–0806). For hcp structured Co crystal phase, the standard peaks indicating the formation of this phase can be seen at 41°, 44°, 47° and 76° corresponding to crystal planes of (100), (002), (101) and (110), respectively (JCPDS card no 05–0727). In the XRD pattern of the CoAuPd/ITO electrode, Co (100) fcc structured Co diffraction plane and Co (200) hcp Co structured Co diffraction plane was observed at 41.9° and 50°, respectively. It is noteworthy mentioning that the synthesis of Co nanostructures that is composed of two phases is already reported.

The nanomorphology of Pd/ITO, AuPd/ITO and CoAuPd/ITO were investigated with SEM as illustrated in Fig. 3 a-c. Also, the morphology of the which demonstrate showing irregular particles across the whole section as shown in Fig. 3a-c. The average particle sizes of these electrodes were estimated as 1500 nm for Pd/ITO, 1500 nm for PdAu/ITO and 2000 nm for CoAuPd/ITO electrode. In addition, large quantities of particulate particles derived from the CoAuPd / ITO rough surface may

be due to the high Pd concentration in solution, as well as in the development of catalytic activities.

Cyclic voltammograms taken in 0.5 M H_2SO_4 for Pd/ITO, AuPd/ITO and CoAuPd/ITO electrodes are shown in Fig. 4. These voltammograms were recorded at 10 mV s^{-1} for these electrodes. The cyclic voltammetric behaviors of bi-metallic AuPd/ITO and CoAuPd/ITO electrodes were evaluated and compared with monometallic Pd/ITO electrode. At present, cyclic voltammogram (CV) of nanoparticles Pd/ITO in 0.5 M H_2SO_4 solution recorded at a scan rate of 10 mV s^{-1} in a wider potential interval from -0.25 to 1V versus Ag/AgCl pseudo reference electrode. Hydrogen reduction / oxidation reaction equilibrium potential is observed at -0.2-0.5 V for Pd/ITO. The cyclic scan shows oxidation/reduction plateaus at the positive anodic potentials and a featureless constant anodic/cathodic current flow region. This is indicative that double layer charging became dominant in the lower potentials of the cyclic scan. Hydrogen peaks emerge at around -0.2 V. The oxidation of Pd commences at above
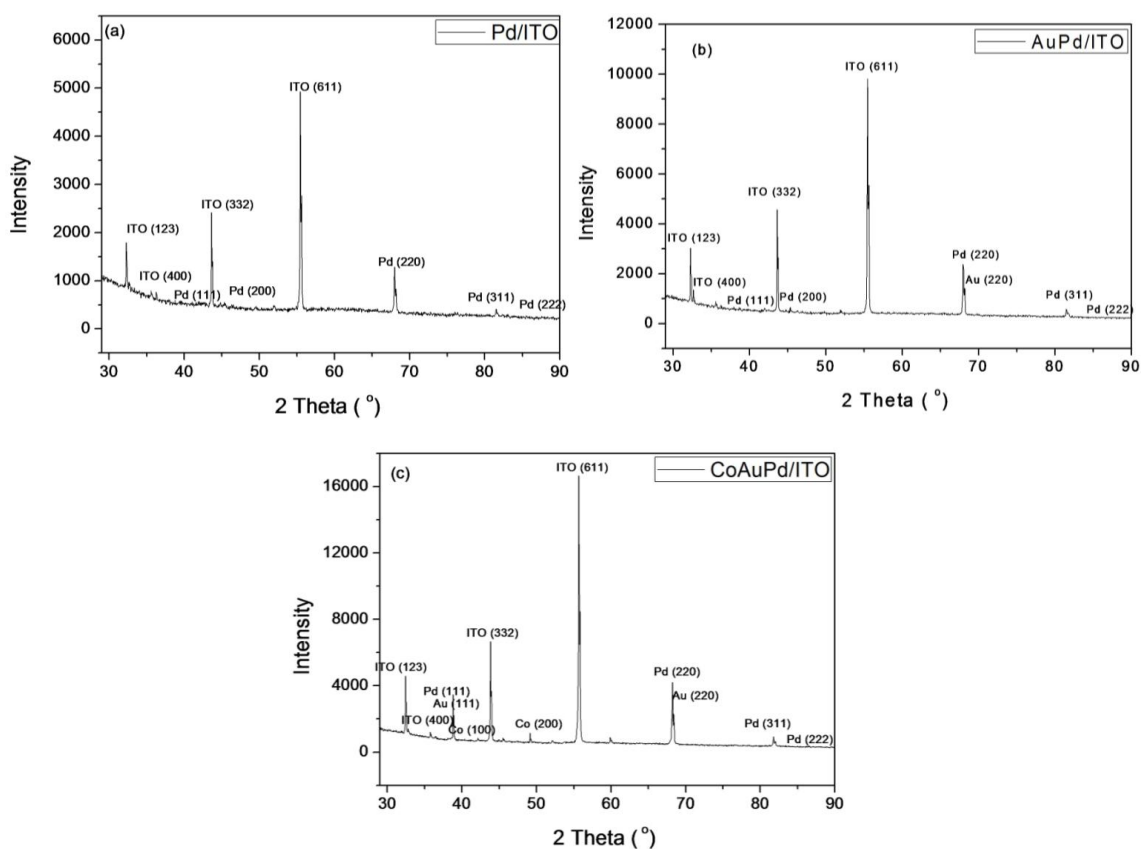
Fig. 2 XRD patterns of (a) Pd/ITO, (b) AuPd/ITO, and (c) CoAuPd/ITO electrodes.

0.5 V. Electrochemical double layer is observed between 0.1-0.5 V. Pd/ITO electrode have very well-defined hydrogen oxidation region (-0.2–0.1 V). Noticeably, these peaks for AuPd/ITO and CoAuPd/ITO electrodes are greater than the ones for Pd/ITO electrode. The area under the hydrogen oxidation region is the greatest for the CoAuPd/ITO electrode, revealing that hydrogen generation is at maximum on this catalyst [9].

Cyclic voltammograms measured in 0.5M H_2SO_4 + 1M HCOOH solution at 10 mV s^{-1} were given in Fig. 5 for Pd/ITO, AuPd/ITO, and CoAuPd/ITO electrodes. For Pd/ITO electrode, the anodic peak around 0.31 V reflects oxidation of FA catalyzed by Pd. One could note that the current value for Pd/ITO electrode is current density value 1.6 10^4 $\mu A/cm^2$ (Current=0.0045 A, and electrode surface area = 0.28 cm^2), which is higher than the one reported in the literature. In a similar study, Kim *et al.* synthesized Pd particles were directly deposited on indium-tin oxide (ITO) electrodes

by cyclic voltammetry (CV). It was observed that current density value for Pd/ITO is 1.6 10^4 $\mu A/cm^2$. Considering cyclic voltammograms taken on Pd/ITO, AuPd/ITO, and CoAuPd/ITO electrodes, the best current value for FAEO was measured for CoAuPd/ITO electrode.

Co and Au addition increases the electrocatalytic activity of FAEO. FAEO maximum forward current corresponding voltages were obtained as 0.31 V for Pd/ITO, 0.15 V for AuPd/ITO, and 0.1 V for CoAuPd/ITO. From these results, it is clear that FAEO occurs at low potentials on CoAuPd/ITO electrode compared to Pd/ITO and CoAuPd/ITO electrodes. This phenomenon is due to the lowest FAEO reaction resistance on CoAuPd/ITO electrode, leading to the highest electrochemical activity.

The catalytic activities and stability of AuPd/ITO and CoAuPd/ITO electrodes were examined by CA technique. Chronoamperomeograms in 0.5 M H_2SO_4 + 1 M HCOOH solution of these
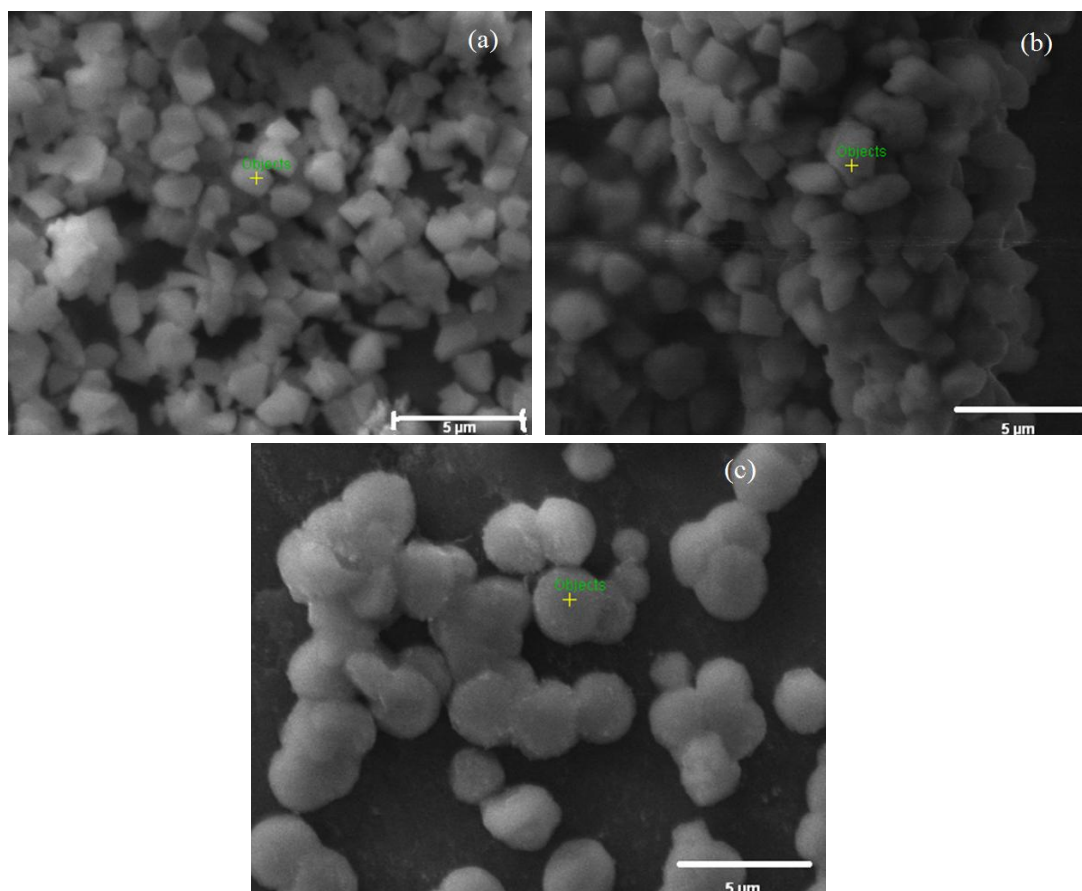

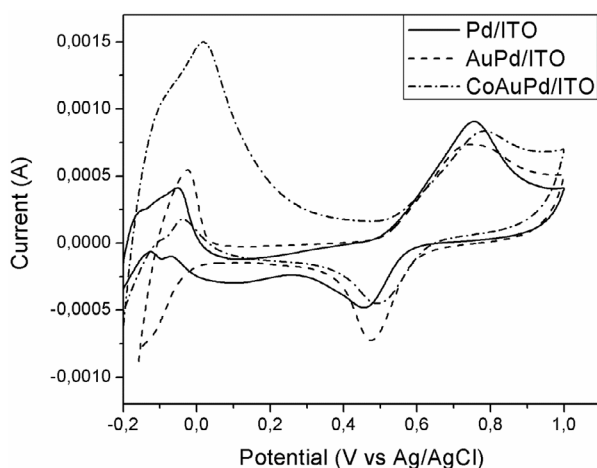Fig. 3: SEM images of (a) Pd/ITO, (b) AuPd/ITO, and (c) CoAuPd/ITO electrodes.

Fig. 4: Cyclic voltammograms of Pd/ITO, AuPd/ITO, and CoAuPd/ITO in 0.5 M H$_2$SO$_4$ at 25.0 °C at scan rate: 10 mV s^{-1}
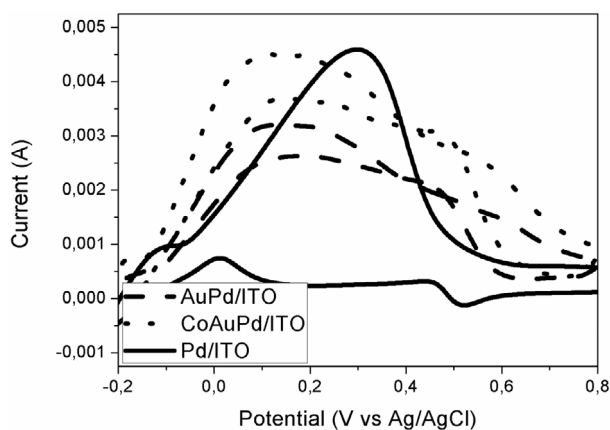(Forward scans were shown).

Fig. 5: Cyclic voltammograms of Pd/ITO, AuPd/ITO, and CoAuPd/ITO in 0.5 M H$_2$SO$_4$ + 1 M HCOOH at 25.0 °C
(scan rate: 10 mV s^{-1}).

electrodes are demonstrated in Fig. 6. There is a continuous current drop for FAEO with time at the initial period because of the accumulation of intermediate and poisonous species at the surface of catalysts, such as CO$_{ads}$, during the oxidation reaction and resulted in the loss of activity [21-22].

CoAuPd/ITO electrode presents higher initial currents compared to the other ones. This could be attributed to the fact that CoAuPd/ITO electrode has a high catalytic activity. On the other hand, lower current decay at the longer time was obtained for CoAuPd/ITO compared to Pd/ITO and AuPd/ITO electrodes, confirming that CoAuPd/ITO electrode has higher electrocatalytic activity, higher resistance to CO, and better long term stability. We have investigated a facile three step electrochemical deposition method for the preparation of CoAuPd on ITO. Besides, Pd and AuPd deposition was performed on ITO by the CV method. The cathodic potential for Pd^{+2} reduction peak shifted more positive potentials for CoAuPd and AuPd compared to Pd, revealing that the electrochemical deposition conditions of Pd^{2+} were changed. For the preparation of Pd/ITO electrode, nucleation and growth of Pd^{2+} were generated only on the surface of the ITO electrodes, having low electrocatalytic activity and low capacitive current. The reduction of Pd^{2+} occurs easily on CoAu/ITO electrode than bare ITO electrode. FAEO measurements indicated that CoAuPd/ITO electrode exhibited higher electrocatalytic activity, higher resistance to CO, and better long-term stability.
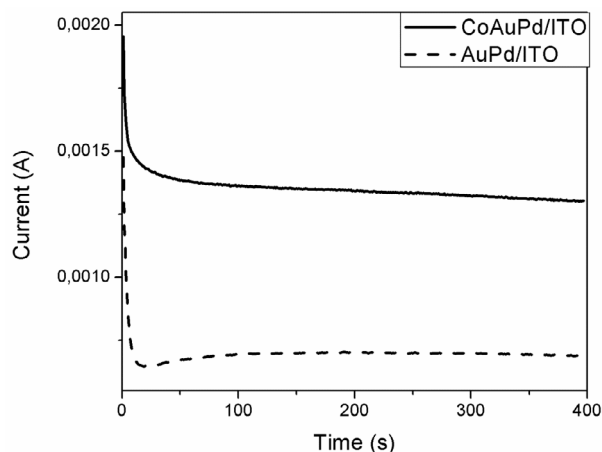
Fig. 6: Chronoamperomograms of Pd/ITO, AuPd/ITO, and CoAuPd/ITO in 0.5 M H$_2$SO$_4$ + 1 M HCOOH at 25.0 °C
(scan rate: 10 mV s^{-1}).

CONCLUSIONS

At present, Pd, PdAu and CoAuPd NPs were successfully fabricated on ITO electrodes by direct electrodeposition. During the electrodeposition process of Pd, PdAu and CoAuPd on to ITO electrode surface, different surface morphologies obtained as presented SEM images. Surface morphology is directly dependent on the electrocatalytic activity, called as structure sensitivity. The results show that CoAuPd/ITO electrode exhibits a better performance and durability for the FAEO to the other Pd and PdAu electrodes. It can be attributed to the synergetic effects of trimetallic catalysts on the FAEO. The presented method seems to be promising for fabricating electrodes for formic acid fuel cells.

ACKNOWLEDGEMENTS

CONFLICT OF INTEREST

The authors declare that there is no conflict of interests regarding the publication of this manuscript.

REFERENCES

[1] Yu X., Pickup P. G., (2011), Screening of PdM and PtM catalysts in a multi-anode direct formic acid fuel cell. *J. Appl. Electrochem.* 41: 589-597.

[2] Ohkubo Y., Shibata M., Kageyama S., Seino S., Nakagawa T., Kugai J., Nitani H., Yamamoto T. A., (2013), Carbon-supported AuPd bimetallic nanoparticles synthesized by high-energy electron beam irradiation for direct formic acid fuel cell. *J. Mater. Sci.* 48: 2142-2150.

[3] Uhm S., Chung S. T., Lee J., (2007), Activity of Pt anode catalyst modified by underpotential deposited Pb in a direct formic acid fuel cell. *Electrochem. Commun.* 9: 2027-2031.

[4] Chen W., Tang Y. W., Bao J. C., Gao Y., Liu C. P., Xing W., Lu T. H., (2007), Study of carbon-supported Au catalyst as the cathodic catalyst in a direct formic acid fuel cell prepared using a polyvinyl alcohol protection method. *J. Power Sources.* 167: 315-318.

[5] Ha S., Adams B., Masel R. I., (2004), A miniature air breathing direct formic acid fuel cell. *J. Power Sources.* 128: 119-124.

[6] Weber M., Wang J. T., Wasmus S., Savinell R. F., (1996), Formic acid oxidation in a polymer electrolyte fuel cell - A real-time mass-spectrometry study. *J. Electrochem. Soc.* 143: L158-L160.

[7] Wang Z. L., Yan J. M., Ping Y., Wang H. L., Zheng W. T., Jiang Q., (2013), An efficient CoAuPd/C catalyst for hydrogen generation from formic acid at room temperature. *Angew. Chem. Int. Ed.* 52: 4406-4409.

[8] Yin M., Li Q., Jensen J. O., Huang Y., Cleemann L. N., Bjerrum N. J., Xing W., (2012), Tungsten carbide promoted Pd and Pd-Co electrocatalysts for formic acid electrooxidation. *Angew. Chem. Int. Ed.* 219: 106-111.

[9] Mehta S. K., Gupta S., (2013), Synthesis of Au-Pd alloy nanoparticles and their catalytic activity in the electrooxidation of formic acid and lower alcohols in alkaline media. *Sci. Adv. Mater.* 5: 1377-1383.

[10] Mikolajczuk A., Borodzinski A., Stobinski L., Kedzierzawski P., Lesiak B., Laszlo K., Jozsef T., Lin H.-M., (2010), Study of Pd-Au/MWCNTs formic acid electrooxidation catalysts. *Phys. Status Solidi. B.* 247: 2717-2721.

[11] Suo Y., Hsing I. M., (2009), Size-controlled synthesis and impedance-based mechanistic understanding of Pd/C nanoparticles for formic acid oxidation. *Electrochim. Acta.* 55**:** 210-217.

[12] Du C. Y., Chen M., Wang W. G., Yin G. P., (2011), Nanoporous PdNi alloy nanowires as highly active catalysts for the electro-oxidation of formic acid. *ACS Appl. Mater. Interf.* 3: 105-109.

[13] Maiyalagan T., Wang X., Manthiram A., (2014), Highly active Pd and Pd-Au nanoparticles supported on functionalized graphene nanoplatelets for enhanced formic acid oxidation. *RSC Advances.* 4: 4028-4033.

[14] Jiang Y. Y., Lu Y. Z., Han D. X., Zhang Q. X., Niu L., (2012), Hollow Ag@Pd core-shell nanotubes as highly active catalysts for the electro-oxidation of formic acid. *Nanotech.* 23: 105609-105615.

[15] Liu X. Y., Dai C. Q., Wu D. F., Fisher A., Liu Z. P., Cheng D. J., (2016), Facile synthesis of PdAgCo trimetallic nanoparticles for formic acid electrochemical oxidation. *Chem. Lett.* 45: 732-734.

[16] Kim B. K., Seo D., Lee J. Y., Song H., Kwak J., (2010), Electrochemical deposition of Pd nanoparticles on indium-tin oxide electrodes and their catalytic properties for formic acid oxidation. *Electrochem. Commun.* 12: 1442-1445.

[17] Tang J., Tian X. C., Pang W. H., Liu Y. Q., Lin J. H., (2012), Co deposition of AuPd bimetallic nanoparticles on to ITO and their electrocatalytic properties for ethanol oxidation.

[18] Agbolaghi S., Nazari M., Zenoozi S., Abbasi F., (2017), The highest power conversion efficiencies in poly(3-hexylthiophene)/fullerene photovoltaic cells modified by rod-coil block copolymers under different annealing conditions. *J. Mater. Sci: Mater. Electron.* 28: 10611–10624.

[19] Agbolaghi S., Abbasi F., Zenoozi S., Nazari M., (2017), Annealing-free multi-thermal techniques comprising aging, cycling and seeding to enhance performance of thick P3HT: PCBM photovoltaic cells via developing hairy crystals. *Mater. Sci. Semicond. Process.* 63: 285-294.

[20] Agbolaghi S., Abbasi F., Gheybi H., (2016), High efficient and stabilized photovoltaics via morphology manipulating in active layer by rod-coil block copolymers comprising different hydrophilic to hydrophobic dielectric blocks. *Europ. Polym. J.* 84: 465–480.

[21] Lepenven R., Levason W., Pletcher D., (1990), Studies of the electrodeposition of palladium from baths based on PD(NH$_3$)$_2$X$_2$ salts. *J. Appl. Electrochem.* 20**:** 399-404.

[22] Li J. D., Tian Q. F., Jiang S. Y., Zhang Y., Wu Y. X., (2016), Electrocatalytic performances of phosphorus doped carbon supported Pd towards formic acid oxidation. *Electrochim. Acta.* 213**:** 21-30.

[23] Miyake H., Okada T., Samjeske G., Osawa M., (2008), Formic acid electrooxidation on Pd in acidic solutions studied by surface-enhanced infrared absorption spectroscopy. *Phys. Chem. Chem. Phys.* 10**:** 3662-3669.

[17] Electrochim. Acta. 81: 8-13.